



CHORUS

This is the accepted manuscript made available via CHORUS. The article has been published as:

Surface roughness noise analysis and comprehensive noise effects on depth-dependent coherence time of NV centers in diamond

P. Chrostoski, P. Kehayias, and D. H. Santamore

Phys. Rev. B **106**, 235311 — Published 14 December 2022

DOI: [10.1103/PhysRevB.106.235311](https://doi.org/10.1103/PhysRevB.106.235311)

Surface roughness noise analysis and comprehensive noise effects on depth-dependent coherence time of NV centers in diamond

P. Chrostoski^{†,*}, P. Kehayias[‡], and D. H. Santamore^{*}

[†]*Sandia National Laboratories, Livermore, California 94550, USA*

[‡]*Sandia National Laboratories, Albuquerque, New Mexico 87123, USA and*

**Department of Physics and Engineering Physics,
Delaware State University, Dover, DE 19901, USA*

(Dated: November 22, 2022)

Noise is a detrimental issue for nitrogen-vacancy (NV) centers in diamond, causing line broadening and decreasing the coherence time (T_2). Following our previous electric and magnetic field noise work, we investigate noise caused by the diamond surface roughness, which is a source for charge density fluctuations and incoherent photon scattering. We find that the varying surface charge density noise source is prevalent throughout the entire NV dynamical decoupling frequency range, while the photon scattering noise is almost negligible. Next, we combine the results from various noise sources to perform comprehensive analyses on T_2 and how it varies with NV depth. At a given NV depth of 5 nm below a hydrogen- or fluorine-terminated surface, we find that these magnetic nuclei reduce the NV coherence time the most, followed by the surface electric field noise sources. The photon scattering and bulk magnetic field noise effects on T_2 are weak compared to the varying charge density, electric dipole, and surface impurity noise. However, with oxygen surface termination, the surface electric field noise sources are comparable to the surface magnetic field noise. Our calculated values of $T_{2,\text{Hahn}}$ (few μs to ten μs) are in good agreement with the experimental values reported elsewhere. Finally, we calculate an anticipated signal-to-noise ratio (SNR) for NV AC magnetometry of external nuclear spins. In our simplified assessment, where some depth-dependent parameters (e.g. NV conversion efficiency) are held constant, we find that shallower NV layers should yield the best SNR, which is consistent with experimental findings.

I. INTRODUCTION

Nitrogen-vacancy (NV) centers in diamond are great candidates for quantum applications, including quantum metrology and sensing, quantum information processing, and hybrid quantum systems [1, 2]. NVs can operate over a wide range of temperatures and environments (including ambient conditions). They also are useful for sensing magnetic fields, electric fields, and temperatures at the nanoscale [3, 4]. When used to sense phenomena external to the diamond, placing NVs close to the diamond surface can improve the signal amplitude and spatial resolution [5–10]. However, shallower NVs experience more surface noise and a faster decoherence rate. This noise broadens the transition linewidths between NV ground-state sublevels, reduces the lifetimes of these sublevels, and decreases the overall quantum sensor performance. Diamond surface noise characteristics are therefore important to understand, since this informs us of the trade-offs between using shallow or deep NVs for external sensing.

Electric and magnetic field fluctuations are major NV noise contributors [11, 12]. Some of the magnetic field noise comes from the nuclear and electronic spin baths in the bulk [13–17]. In addition, the diamond surface also contributes noise due to electron spins of dangling bonds [18, 19], terminating surface atoms [20, 21], adsorption of external molecules [22], and static magnetic impurities in thin films [23, 24]. Static magnetic impurities can arise within the bulk naturally or on the surface in thin films, and have been experimentally observed for both bulk and single-crystal surfaces [14, 25, 26].

In our previous work, we showed that the terminating surface atoms (hydrogen, fluorine, and oxygen) often used in experiments can generate more magnetic field noise than the magnetic impurities (^{13}C nuclei) within the bulk [27]. We also showed that the electric dipole fluctuations of the diamond surface and different protective surface layers are a large source of surface electric field noise [28]. Electric field noise is important, as it causes population decay between the NV $|+1\rangle$ and $|-1\rangle$ ground-state sublevels [11] and decoherence for Autler-Townes dressed states for divacancy defects in 4H-SiC [29]. Another significant electric field noise source comes from the diamond surface roughness. A recent experiment found that tri-acid cleaning and oxygen annealing led to a $4\times$ increase in shallow NV coherence times [30]. Until now there has been no systematic theoretical study of electric field noise due to the rough surface in NV quantum sensors. Taking a comprehensive noise approach and analyzing the noise source contributions to NV coherence time is crucial to improve quantum sensing with shallow NVs.

In this paper, we have two objectives: (a) calculate the noise generated by the rough diamond surface, and (b) provide a comprehensive approach of determining how noise sources affect coherence time by including all other noise sources from previous work, and investigate the optimized NV depth.

For rough-surface noise, we study two mechanisms: varying surface charge distribution fluctuations and photon scattering. A trough created by the rough surface will trap free surface electrons. The amount of trapped charge varies among the troughs, causing charge distribu-

tion fluctuations that lead to noise. We model the noise due to the varying charge density using the Schottky approximation, and generate the noise spectrum by using trapped charge density statistics [31] (see Sec. II A.)

The optical and microwave photons from the NV initialization, readout, and dynamical decoupling pulses will scatter due to elastic collisions with atoms in the diamond substrate. The atoms then vibrate, emitting electromagnetic radiation. To model the photon scattering, we consider incoherent scattering due to the non-flat rough surface. We use the Green's function method along with a Gaussian rough surface correlation to determine the scattering field which will interact with the NV electron spin. With the scattering field two-time correlation determined, the Wiener-Khinchin theorem [32] yields the noise power spectrum (see Sec. II B).

In Sec. III we investigate all noise sources present from previous work [27, 28] and this current rough-surface work to calculate their effect on the inhomogeneous dephasing time T_2^* . We use the Gaussian phase noise approximation [33, 34] that relates the Hahn echo coherence time ($T_{2,\text{Hahn}}$) with the noise when it has reached a white noise spectrum. We also calculate the surface noise effect on the longitudinal relaxation time T_1 by applying Fermi's Golden Rule for electrical dipole interaction noise [35], as described in Sec. III A 2. After determining $T_{2,\text{Hahn}}$ and T_1 , we can determine T_2^* through the inverse relationship between T_2^* , $T_{2,\text{Hahn}}$, and T_1 .

Recent experiments have seen that NV lifetimes depend on depth [12, 36, 37]. In Sec. IV, we find the depth dependence of the NV $T_{2,\text{Hahn}}$ and T_1 lifetimes. We then calculate the magnetic sensitivity to AC magnetic fields (η) and the magnetic field variance from Larmor precession of external nuclei on the diamond surface (B_{RMS}^2), which is the signal strength for NV NMR spectroscopy. These two factors, η and B_{RMS}^2 , both contribute to the NV NMR spectroscopy signal-noise-ratio (SNR), and they have opposite depth dependence: η improves with deeper depth while B_{RMS}^2 improves with shallower depth. We then predict how the SNR for detecting external solid-state nuclei with a shallow NV varies with depth, as was done experimentally in Ref. [38] for ^{11}B in hBN.

The work presented here shows that the surface noise plays a major role in reducing the coherence times of shallow NVs. By understanding and mitigating this noise, extending the lifetimes for shallow NVs, and determining an optimal NV depth for external sensing, one could improve the sensitivity of a wide range of NV sensing applications.

II. SURFACE ROUGHNESS NOISE MODELS AND RESULTS

To calculate the rough surface noise, we first identify two noise mechanisms. The first mechanism is due to rough surface defects (which in diamond are usually pri-

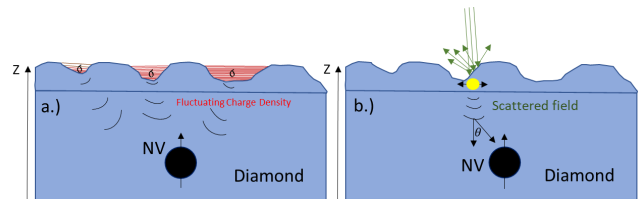


FIG. 1. Rough surface model for a) valleys creating areas where electrons can collect and become trapped generating a varying charge density per unit area due to electrons fluctuating as they repel and try to escape. The rough surface also gives b) incoherent photon scattering where the scattered atom will begin to oscillate based on the incident pulse from either an initialization and readout or dynamical decoupling microwave pulse.

mal $C = C \text{ sp}^2$ bonds [39]) trapping electrons (see Fig. 1). Depending on the defect shapes and sizes, some regions have more trapped electrons than others, causing charge density variations along the surface that leads to time-dependent fluctuations of the charge density (see Sec. II A). The second mechanism is the rough surface causing incoherent scattering of the laser initialization, readout, and dynamical decoupling microwave pulses, causing photon intensity fluctuations (see Sec. II B). NVs experience the electric fields from these sources, which enter the NV Hamiltonian as

$$H = d_{\parallel} E_z \left[S_z^2 - \frac{2}{3} \right] - d_{\perp} \left[E_x (S_x S_y + S_y S_x) + E_y (S_x^2 - S_y^2) \right], \quad (1)$$

where $d_{\parallel,\perp}$ are the coupling strengths, \mathbf{E} is the electric field, and $S_{x,y,z}$ are the NV electron spin operators.

The surface roughness (Ra) of Element Six (E6) chemical vapor deposition (CVD) diamonds commonly used in many experimental setups is 5 nm after polishing. E6 can use scaife polishing to smooth the diamond surface to an Ra as small as ≤ 1 nm [40].

A. Rough surface charge distribution noise

To determine the noise spectral density due to the varying charge density, we use the Schottky approximation to determine the total charge per unit area (see Ref. [39] for an approximate solution similar to our direct derivation),

$$Q_d = \sqrt{q N_A 2 \varepsilon \varepsilon_0 (E_F - E_n)}. \quad (2)$$

Here, ε is the relative permittivity of diamond, ε_0 is the permittivity of free space, q is the electron charge, N_A is the defect concentration, E_F is the Fermi energy level, and E_n is the local energy level within the defect region.

Using the total areal charge due to the surface defects, we now consider the time-dependent charge concentration as the troughs trap surface charges. Xia *et*

al. [31] showed that the time-dependent charge concentration due to trapped electrons is

$$\sigma(t) = qN_{\text{trap}}f(E_n)\exp\left[-\frac{v_{\text{de}}^2 t^2}{2}\right]. \quad (3)$$

Here q , N_{trap} , and $f(E_n)$, are the electron charge, number of trapped electrons, and Fermi-Dirac distribution function at $t = 0$, respectively, and $v_{\text{de}} = (k_B T)^3 / (6h^3 v^2)$. Furthermore, v_{de} is the maximum detrapping rate, k_B is Boltzmann's constant, T is temperature, h is Planck's constant, and v is the orthogonal vibrational frequency around the defect. The energy level of the traps (i.e. the Fermi level pinning) is temperature- and time-dependent, and is represented by $E_T = k_B T \ln(v_{\text{de}} t)$. Assuming that q is the total charge at $t = 0$, and Eq. (3) is for the concentration of charge, q will now be replaced by the total charge per unit area due to the defects causing roughness, $Q_d = \sqrt{qN_A 2\epsilon\epsilon_0(E_F - E_n)}$. Plugging in the total charge per unit area (Eqn. (2)) and the Fermi-Dirac distribution function will give a time-dependent charge density (see Appendix (A 1)).

With the time dependence of the charge density, the two-time correlation can be expressed by an autocorrelation function of the time-dependent charge density, which can be plugged into the Wiener-Khinchin theorem to determine the noise spectral density,

$$S_{CD}(\omega) = \int_{-\infty}^{\infty} \langle \delta\sigma(t), \delta\sigma(t + \tau) \rangle \exp[-i\omega\tau] d\tau. \quad (4)$$

After applying the Wiener-Khinchin theorem, we get the noise power density,

$$S_{CD}(\omega) = Q_d^2 N_{\text{trap}}^2 f(E_n)^2 \frac{\exp\left[-\frac{\omega^2}{v_{\text{de}}^2}\right]}{v_{\text{de}}^2} \sqrt{2\pi}. \quad (5)$$

B. Photon scattering noise

As photons from the initialization, readout, and dynamical decoupling pulses interact with the diamond substrate, atoms within the diamond will have elastic collisions with incoming photons. The atoms will vibrate, emitting electromagnetic radiation. The noise generated from the elastic scattering requires knowing the fields radiated from the scattering. We approach this by considering the Green's function method applied to the wave equation as described in the appendix (A 2). The scattered field due to the incoherent scattering of the rough surface can be described by the following electric field,

$$E(t) = \frac{qa(t)\sin(\theta)}{4\pi\epsilon_0 r c^2}. \quad (6)$$

Here q is the electron charge, r is the radial distance from the electron, $a(t)$ is the vibrational acceleration of the scattered atom, θ is the scattering angle, and c is

the speed of light. We now create a two-time correlation function and apply the Wiener-Khinchin theorem to relate to the noise spectral density,

$$S_{RS}(\omega) = \int_0^{\infty} \langle E(t)E(t + \tau) \rangle \exp[-i\omega\tau] d\tau, \quad (7)$$

$$S_{RS}(\omega) = E(\theta)^2 \frac{1}{2\omega_{\text{inc}}(\omega_{\text{inc}} + \omega)}. \quad (8)$$

Here $E(\theta)^2 = \frac{q^2 E_0 \sin(\theta)}{m_e 4\pi\epsilon_0 r c^2}$ and m_e is the electron mass.

To characterize the rough surface causing photon scattering, we need a correlation function that describes the surface roughness. We describe the rough surface correlation as follows,

$$C(R) = \frac{1}{\sigma^2} \langle h(r)h(r + R) \rangle, \quad (9)$$

where $h(r)$ is the surface height a distance r away from a smooth reference plane and σ is the root-mean-square height. We use Gaussian height distributions as they are widely used to describe rough surfaces. If we consider the rough surface heights that arise from a large number of random local defects, we can use the central limit theorem to have the cumulative effect be described using a Gaussian function. To see how the surface roughness affects the noise due to scattering, we generate the power spectrum of the rough surface by taking the Fourier transform to get the rough surface power density,

$$P_G(\omega) = \frac{\sigma^2 \lambda}{4\pi^{3/2}} \exp\left(\frac{\lambda^2 \omega^2}{4c^2}\right). \quad (10)$$

Here ω/c is related to the wave number through $k = \omega/c$, and λ is the correlation length (which relates to the surface roughness Ra). Now that we have the rough surface noise power spectrum, we need to combine our noise and rough surface power densities to generate the actual photon scattering noise power spectral density seen by the NV spin, giving us the following

$$S_{RS}(\omega) = P_G(\omega)E(\theta)^2 \frac{1}{2\omega_{\text{inc}}(\omega_{\text{inc}} + \omega)}, \quad (11)$$

where ω_{inc} is the incident photon frequency.

C. Results and discussion - rough surface noise

NV dynamical decoupling experiments often probe the $10^3 - 10^7$ Hz operational frequency range, though NVs can also sense higher frequencies when measuring Rabi frequencies or T_1 lifetimes. We initially calculated the noise spectrum from the varying charge density due to the rough surface for this range, but noticed that the noise very quickly reaches its maximum, making it nearly constant throughout the operational frequency range. To see any changes, we expanded the frequency range (see

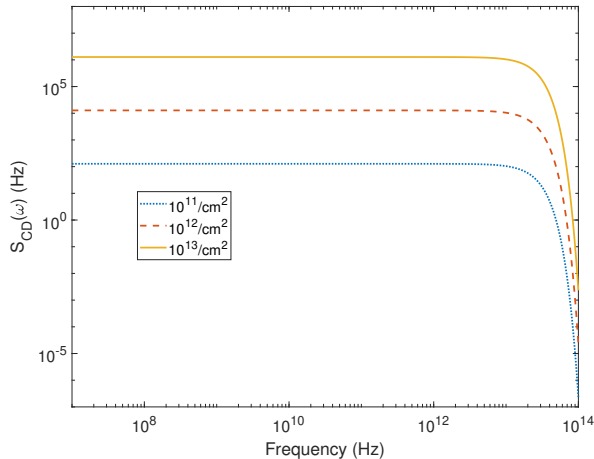


FIG. 2. Noise power spectra for varying charge distribution noise when considering a concentration of $10^{13}/\text{cm}^2$ (orange dotted), $10^{12}/\text{cm}^2$ (red dashed), $10^{11}/\text{cm}^2$ (blue) trapped charge area density. A $10^{13}/\text{cm}^2$ surface charge density is a plausible trapped charge area density due to surface defects [39] before any polishing.

Fig. 2). This almost-constant noise amplitude within the operational frequency range is associated with the fact that it does not take many electrons getting trapped to start interacting with each other and vibrate rapidly, generating noise. The noise amplitude also depends on the square of the electron density trying to escape from the troughs. The more electrons interacting within the troughs, the more noise will be generated.

As the surface becomes smooth, the charge density on the surface becomes more uniform, leading to a large decrease in electrons being trapped in troughs, reducing the noise. This leads to a smaller noise floor maximum for a smoother surface, but it does not take many electrons getting trapped in troughs to start interacting with each other, meaning the noise is present throughout the entire operational frequency range. Thus, smoothing out the surface by successive tri-acid cleaning and annealing is effective in reducing the surface noise [30].

To calculate the noise for the initialization and readout laser pulses and the dynamical decoupling microwave pulses, the scattering field was set normal to the NV axis to make the $E(\theta)$ term maximum. This setup allows us to study the frequency dependence of the noise spectra in addition to studying its worst-case scenario. Figure 3 shows the noise spectrum for the initialization and readout laser pulses. We considered a 285 mW initialization and readout laser power, $10 \mu\text{s}$ pulse duration, and a $40 \mu\text{m}$ diameter laser spot size (intensity $I = 23 \text{ kW}/\text{cm}^2$). [38]. We also considered several reported NV optical saturation intensities, due to disagreement in the literature [41–43]. The laser pulses have several orders of magnitude larger noise amplitude than the dynamical decoupling pulses. This is because the laser pulse electric field amplitudes are much larger than those

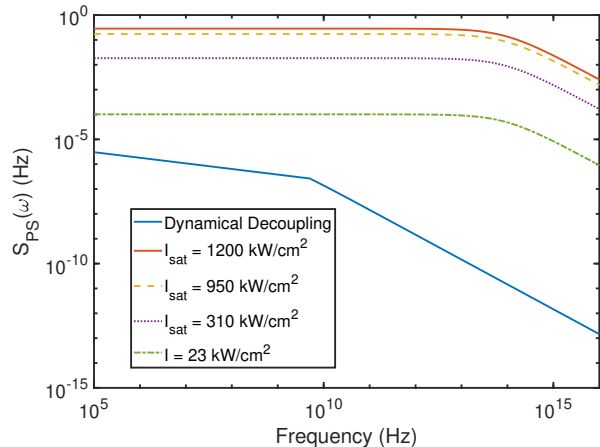


FIG. 3. Noise power spectra from photon scattering of the initialization and readout laser pulses at the NV optical saturation intensity $I_{\text{sat}} = \frac{hc}{\lambda\sigma\tau}$, where $\lambda = 532 \text{ nm}$ is the pump laser wavelength, σ is the NV absorption cross section at 532 nm, and $\tau \approx 10 \text{ ns}$ is the upper-state lifetime. Since there is disagreement in the literature for the value of σ , here we show the results for $\sigma = 2.4 \times 10^{-17} \text{ cm}^2$ ($I_{\text{sat}} = 1200 \text{ kW}/\text{cm}^2$, red solid) [41], $\sigma = 3.1 \times 10^{-17} \text{ cm}^2$ ($I_{\text{sat}} = 950 \text{ kW}/\text{cm}^2$, orange dashed) [42], and $\sigma = 9.5 \times 10^{-17} \text{ cm}^2$ ($I_{\text{sat}} = 310 \text{ kW}/\text{cm}^2$, purple dotted) [43], and the experimental setup of Henshaw et al. [38] ($I = 23 \text{ kW}/\text{cm}^2$, green dashed-dotted).

of the dynamical decoupling microwave pulses (typically $\sim 10 \text{ W}$ microwave power and $\sim 30 \text{ ns}$ pulse duration). The peak field amplitude differences in the pulses leads to the acceleration of the scattered atoms being much larger for the laser pulses. We also studied varying the rough surface correlation length from values ranging near the Van der Waals radius for carbon (0.17 nm) to a few millimeters (a typical diamond size), and saw no change in the noise amplitude. This indicates that the pulses do not notice the rough surface. Unfortunately, smoothing the surface does not reduce the noise from photon scattering (like for the varying charge density). On the other hand, noise during the laser pulses shouldn't affect the NV lifetimes since they are being optically pumped. In addition, if the NVs undergo most of their phase accumulation (and decoherence) in the time between microwave pulses during a dynamical decoupling AC magnetometry experiment, additional noise during the microwave pulses also shouldn't matter much (see Section (IV A)).

The noise power spectra due to laser pulses and microwave pulses (Fig. 3) and microwave pulses resemble low-pass filters, though with different cutoff frequencies ($\sim 5 \times 10^{13} \text{ Hz}$ compared to $\sim 5 \times 10^9 \text{ Hz}$). The laser pulse noise cutoff frequency is beyond the practical NV AC magnetometry frequency range, meaning it's essentially white noise. The microwave pulse noise could be reduced for NV AC magnetometry experiments that surpass this cutoff frequency with an appreciable bias magnetic field. Also note that the mi-

crowave pulse noise power spectrum isn't flat below the cutoff frequency. Finally, NV AC magnetometry experiments should filter out much of this white noise, though the filter pass-bands will still allow some noise through.

We see different power laws for the microwave pulse and laser pulse noise power spectra (Fig. 3 and 4). For the microwave pulse noise, we see a $1/f$ power law at high frequencies. This makes sense as we consider that the photon will scatter off a charged particle within the diamond. This type of scattering will lead to a $1/f$ noise power law [44–46]. For the laser pulse noise, we see a $1/f^2$ power law at high frequencies. This type of noise can come from a generation-recombination mechanism [47]. This makes sense for the case of the initialization pulse as the NV will absorb the energy and release it through photon emission.

With the noise spectra for the varying charge density and photon scattering determined, we can compare all of the surface noise effects we have studied so far. Fig. 4 shows the noise contributions from each of the surface noise models we have studied so far. We assume an oxygen-terminated surface without a protective dielectric layer, and a surface roughness that gives a $10^{13}/\text{cm}^2$ trapped charge density. This allows us to study a plausible scenario of the surface noise present in a given experiment before much noise mitigation has been done. For frequencies < 1 kHz (not shown), the electric dipole noise is the largest noise source. Continuing to look at the lower frequencies, the electric dipole and varying charge noise density are the largest noise sources. The next largest noise source is the oxygen surface impurity magnetic noise, followed by the photon scattering noise of the initialization and readout pulses when considering the $23 \text{ kW}/\text{cm}^2$ laser intensity of Henshaw *et al.* [38]. The smallest surface noise contribution is from the dynamical decoupling microwave pulses, which makes sense when considering the small intensity of the pulses causing a low photon scattering noise floor. These noise profiles will vary based on experimental details, but this gives insight into a scenario for an experiment with limited mitigation done.

III. COMPREHENSIVE NOISE EFFECTS ON COHERENCE TIMES AND DEVICE SENSITIVITY

A. Coherence time - noise relationship

With our previous work on electric- and magnetic-field noise [27, 28] and current work on rough surface noise, we can now take a comprehensive approach to noise effects on shallow NVs.

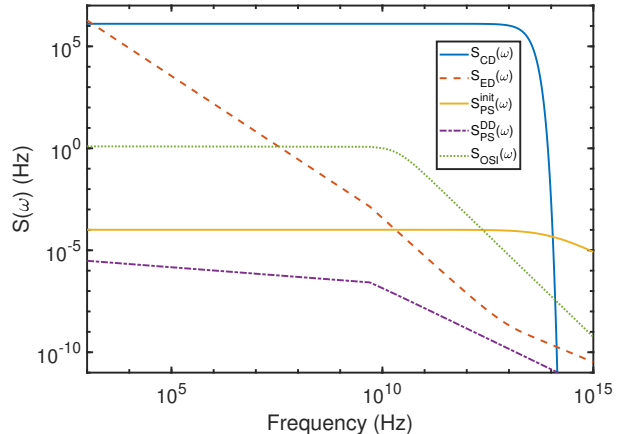


FIG. 4. Noise power spectra for various surface noise sources considering a 5 nm NV depth, including electric dipole noise considering a bare diamond surface ($S_{ED}(\omega)$, red dashed), varying charge density ($S_{CD}(\omega)$, blue solid), photon scattering from the initialization and readout beams ($S_{PS}^{init}(\omega)$, orange solid), photon scattering from the dynamical decoupling pulses ($S_{PS}^{DD}(\omega)$, purple dashed-dotted), and the magnetic surface impurity noise from oxygen termination ($S_{OSI}(\omega)$ green dotted).

1. Gaussian phase-noise approximation of $T_{2,\text{Hahn}}$

Our task is to examine how noise from all these different sources affects the NV coherence time, $T_{2,\text{Hahn}}$. We assume that the fluctuations will obey Gaussian statistics [33, 34], i.e. that the probability distribution for the stochastic phase of the NV system will follow a Gaussian

$$p(\varphi) = \frac{1}{\sqrt{2\pi \langle \varphi^2 \rangle}} \exp\left(-\frac{\varphi^2}{2 \langle \varphi^2 \rangle}\right), \quad (12)$$

where φ is the stochastic phase of the NV. To be more specific, we consider an NV with Bloch vector \mathbf{M} plugged into the Schrödinger equation, giving $\dot{\mathbf{M}} = \mathbf{B} \times \mathbf{M}$, where \mathbf{B} is the magnetic field. The magnetic field here will have a static part and a stochastic part, which splits the total phase, ϕ , into the sum the regular phase, ϕ_0 , and the stochastic phase.

In the Gaussian approximation, the only relevant statistical characteristic is the two-time correlator of the random fluctuation $\langle v(t), v(t + \tau) \rangle = W(|t - \tau|)$, where v is a random variable. $W(|t - \tau|)$ vanishes as $\tau \rightarrow \infty$. The integration time will be much larger than the decay of the correlation function, thus, the central limit theorem becomes applicable and is independent of the details of the process. The stochastic phase decay is then given by

$$e^{-\frac{t}{T_2}} = \int p(\varphi) e^{i\varphi} d\varphi = e^{-\frac{1}{2} \langle \varphi^2 \rangle}. \quad (13)$$

Here t is the integration time and $\langle \varphi^2 \rangle$ is the phase vari-

ance. The power spectrum of the noise $S(\omega)$ is

$$S(\omega) = \frac{1}{\pi} \int_0^\infty W(t) \cos(\omega t) dt. \quad (14)$$

Combining Eq. (12) with Eq. (14) yields the following relation

$$\langle \varphi^2 \rangle = 4 \int_{-\infty}^\infty \frac{\sin^2(\frac{\omega t}{2})}{\omega^2} S(\omega) d\omega. \quad (15)$$

For large t , it becomes

$$\langle \varphi^2 \rangle = 2\pi t S(0). \quad (16)$$

The coherence time relates to the noise at its maximum value ($S(\omega \rightarrow 0)$),

$$T_{2,\text{Hahn}} = \frac{1}{\pi S(0)}. \quad (17)$$

2. T_2^* , $T_{2,\text{Hahn}}$, and T_1 noise

Next, we determine how each noise source contributes to T_2^* , $T_{2,\text{Hahn}}$, and T_1 decay. We have modeled each noise source independently so we can relate the inhomogeneous dephasing time with the coherence time predicted from each noise source. We follow the T_2^* expression as given in Ref. [4],

$$\frac{1}{T_2^*} \approx \frac{1}{T_2^{\text{elect}}} + \frac{1}{T_2^{\text{mag}}} + \frac{1}{T_2^{\text{other}}} + \frac{1}{2T_1}, \quad (18)$$

with

$$\frac{1}{T_2^{\text{elect}}} = \frac{1}{T_2^{\text{dip}}} + \frac{1}{T_2^{\text{CD}}} + \frac{1}{T_2^{\text{PS}}}, \quad (19)$$

$$\frac{1}{T_2^{\text{mag}}} = \frac{1}{T_2^{\text{surf}}} + \frac{1}{T_2^{\text{bulk}}}. \quad (20)$$

Here T_2^{elect} encompasses the predicted $T_{2,\text{Hahn}}$ for the electric field noise sources (electric surface dipoles T_2^{dip} , photon scattering T_2^{PS} , and varying surface charge density T_2^{CD}), while T_2^{mag} encompasses the predicted $T_{2,\text{Hahn}}$ for the magnetic field noise sources (electronic surface spin bath T_2^{surf} and nuclear spin bath T_2^{bulk}) and the longitudinal relaxation time of the NV, T_1 . To get a full prediction of T_2^* , other sources that affect the inhomogeneous dephasing time such as strain effects and other possibly unknown effects will also need to be incorporated. However, they are out of the scope of this work so we will focus only on how the various noise profiles we have modeled effect the coherence time. Experiments have also shown that the Hahn echo pulse technique can yield a $T_{2,\text{Hahn}}$ lifetime much longer than T_2^* [4, 5, 48–50].

Determining T_1 is done by considering the interaction Hamiltonian Eq. (1). If the system is placed close to polar molecules or dielectric materials, electrical noise from

the surface will couple the $|1\rangle$ and $|-1\rangle$ states together and cause transitions between these states. The rate of this relaxation can be written using Fermi's Golden Rule [35],

$$\frac{1}{T_1} = \frac{d_1^2}{2} \coth\left(\frac{\beta\omega}{2}\right) \int_{-\infty}^\infty \langle [E(t), E(0)] \rangle e^{-i\omega t} dt + \frac{1}{T_1^{\text{phon}}}. \quad (21)$$

Here $\beta = 1/k_B T$, $\langle [E(t), E(0)] \rangle$ is the thermally-averaged auto-correlation function, and $1/T_1^{\text{phon}}$ encompasses the bulk relaxation rate due to phonons [51], including the possibility of surface phonon effects. The Fourier transform in Eqn. (21) includes the electric field noise from an electric dipole interaction with a surface dielectric. We have modeled the electric dipole noise due to surface dielectrics previously [28] allowing us to use our previous model to predict the dipole noise effect on T_1 and get a gauge on T_2^* based on different experimental setups.

3. NV relaxation depth dependence due to various noise sources

Recent experiments have reported how $T_{2,\text{Hahn}}$ depends on the NV depth d , and the optimal depths for various experimental situations [12, 36–38]. Equation (17) and our work support the experimental observations: from our previous work on electric dipole noise [28], we found that the electric dipole noise had a $1/d^2$ dependence. From Eqns. (A4) and (8) there is also a $1/d^2$ dependence on rough surface noise for both the varying charge density and photon scattering noises. On the other hand, for the magnetic noise due to impurity spins at the surface, the magnetic dipole moment spin-spin interactions give a $1/d^3$ dependence [27]. Finally, for the bulk impurity spins, the spin-spin magnetic dipole moment interaction depends on the distance between the NV and the ^{13}C nuclear spin bath, which is on the order of 0.44 nm for natural-abundance ^{13}C (1.1%) [52]. In this sense, there is no real depth dependence as the bulk noise will be felt before any surface effects. Similar to the $T_{2,\text{Hahn}}$ depth dependence being driven by the noise, T_1 also has a depth dependence as it is affected by the electric dipole noise. We discuss the depth dependence in details in Sec. IV.

IV. RESULTS AND DISCUSSION - NOISE EFFECT ON NV LIFETIMES

A. Noise effect on T_2 coherence time

In this section, we calculate the depth-dependent $T_{2,\text{Hahn}}$ coherence time (or decoherence rate) for each noise source using the results from the previous work [27, 28] and the ones obtained in Sec. II C. For noise spectrum calculations of electric and magnetic field noise, we

refer to our previous work [27, 28]. Then, we compare their effects on $T_{2,\text{Hahn}}$. Table (I) shows the coherence time at a depth of 5 nm for each noise source. We did not include the bulk magnetic field noise (e.g. ^{13}C and substitutional nitrogen) since it does not have a clear depth dependence and would obscure the comparison of other noise effects. We see that the hydrogen- and fluorine-terminated surface impurity magnetic field noise sources give the shortest $T_{2,\text{Hahn}}$ time. This is due to the $1/d^3$ dependence compared to the $1/d^2$ dependence for the surface electric field noise.

Noise Source	Coherence Time (μs)
Electric dipole (BD)	3.9
Electric dipole (glyc)	22.5
Electric dipole (PC)	30.8
Varying charge density	4.42
Photon scattering	10^4
Surface nuclei (F)	0.004
Surface nuclei (H)	0.08
Surface nuclei (O)	10^5

TABLE I. Coherence time effects when considering a 5 nm depth from electric dipole noise when considering bare diamond (BD), glycerin covering layer (glyc), and propylene carbonate covering layer (PC), varying charge density noise, photon scattering noise from the initialization and readout pulses with $I_{\text{sat}} = 1200 \text{ kW/cm}^2$, and magnetic surface impurities of terminating atoms fluorine (F), hydrogen (H), and oxygen (O).

The oxygen-terminated surface (which is a widely-used method to get rid of dangling bonds on the surface) gave a much longer $T_{2,\text{Hahn}}$ time compared to the electric field noise effects. The depth proportionality difference of electric field noise and magnetic field noise may explain why the work by Myers *et al.* [12] shows the electric field noise at the surface being comparable to the magnetic field noise. In their work, they attempt to decompose the noise spectrum into electric field noise and magnetic field noise since they use the magnetic field variance proportional to $1/d^2$ rather than $1/d^3$.

The surface electric dipole contaminations with no protective cover layer and rough surface with the varying charge density electric field noise gave the next shortest $T_{2,\text{Hahn}}$ times. When looking at glycerin and propylene carbonate protective layered electric dipole noise, we see an order of magnitude increase in the $T_{2,\text{Hahn}}$ time which supports previous claims that choosing the correct protective layer is important. The initialization and readout pulse photon scattering noise and oxygen-terminated surface impurity magnetic field noise give the longest $T_{2,\text{Hahn}}$ times due to their overall addition being masked due to the other stronger noise sources. As expected, the microwave dynamical decoupling pulses (not included in the table) will also not contribute much to the $T_{2,\text{Hahn}}$ decay rate.

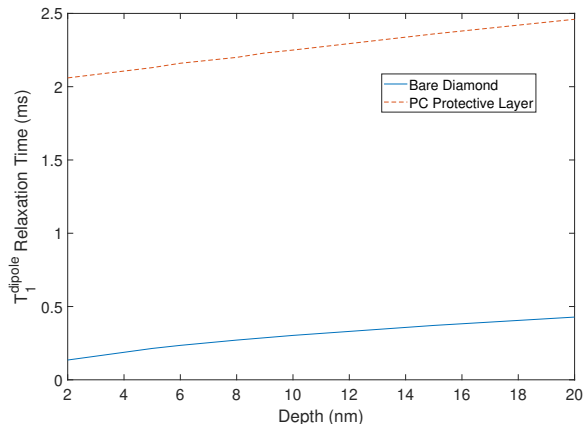


FIG. 5. T_1^{dipole} relaxation times when considering a bare diamond electric dipole noise (blue line) and a protective layer of propylene carbonate (PC) (dashed red line). These values are consistent with the few-ms T_1 seen in experiment, though the bulk T_1 lifetime is also a few ms.

B. T_1 and T_2^* calculations

NV relaxometry experiments have shown that NV room-temperature T_1 times are a few milliseconds, depending on the depth [11, 12, 51]. **From Eqn. (21) we see that one part of the T_1 depth dependence comes from the electric dipole noise. It should be noted that the T_1^{phon} piece will have a depth dependence of its own. In Fig. 5 we calculate T_1 times due to the surface electric dipole noise at different depths (denoted T_1^{dipole}) to compare to experimentally-determined values.** We look at the cases of a bare diamond surface and a propylene carbonate (PC) protective layer, as this will change the electric dipole interaction strength. Our calculations for T_1 come out on the order of a fraction of a millisecond for the bare diamond and a few milliseconds with a PC protective layer. These values show good agreement with measured values in the few-millisecond range as seen by Myers *et al.* [11, 12]. Note that the bulk T_1 lifetime (due to phonons) is also a few milliseconds [51].

With the $T_{2,\text{Hahn}}$ decay rates from the different noise sources and T_1 determined for different depths, we now use equation (18) to calculate T_2^* . Looking at Eq. (18), we can see that T_1 affects T_2^* minimally, as T_1 is typically much longer than the T_2^* contributions from the other noise sources.

As mentioned in the previous section, dynamical decoupling pulse sequences can extend the NV coherence times based on the number of π -pulses N . **Experimental observations have shown that T_2 should improve with N as $T_{2,N} = N^{2/3}T_{2,\text{Hahn}}$, including for shallow NV layers [53], and we use the same $N^{2/3}$ scaling here.** For $N = 48$ pulses, we get $T_{2,48}$ values of tens of μs for depths of 2 – 10 nm and $\sim 100 \mu\text{s}$ for 20 nm

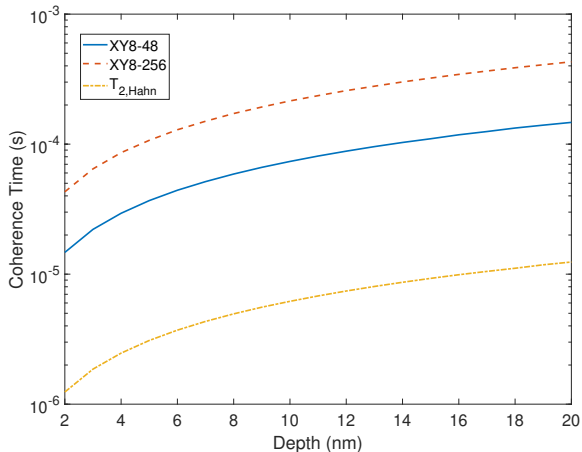


FIG. 6. NV coherence times for XY8-48 (solid blue line), XY8-256 (dashed red line), and Hahn echo (dashed-dotted orange line) as a function of depth. The coherence time improves with depth d , as the surface magnetic field noise is proportional to $1/d^3$ and the surface electric field noise is proportional to $1/d^2$.

depths, which are in good agreement with experimental observations (see Fig. 6). For $N = 256$ pulses, we saw coherence times as long as hundreds of μs . Note that we are only considering the noise effects on T_2 which we have modeled so far; there may be other effects present (e.g. strain fluctuations) which can accelerate the decoherence process. Nevertheless, our calculations tell us that these noise sources are playing a big part in decreasing coherence times with surface noise playing a large role. Being able to use methods to mitigate the noise from these different sources will be important to extend these coherence times even further. Some of the suggestions to reduce electric dipole noise are discussed in our previous work [28].

C. Depth optimization for NV NMR spectroscopy

In NV NMR spectroscopy of statistically-polarized external nuclei, two parameters are critical: the magnetic sensitivity and the nuclear magnetic field amplitude. The sensitivity η is the minimum B_{RMS}^2 magnetic field noise amplitude that can be measured in a fixed amount of measurement time. η is related to T_2 in the following way:

$$\eta \approx \frac{\pi^2 e \sqrt{T_2 + T_R}}{\gamma_e^2 T_2^2 A \sqrt{I_{PL} t_{int}}}, \quad (22)$$

where γ_e is the electron gyromagnetic ratio (in MHz/T), I_{PL} is the photon count rate in photons/s, A is the photoluminescence spin contrast, t_{int} is the readout signal integration time, and T_R is the total readout and initialization time. Here we assume that the noise floor

improves with the square root of the experimental averaging time. Since the sensitivity contains T_2 , it has a depth dependence, which we calculate below. For simplicity, we consider the sensitivity of a single NV rather than an ensemble, since the depth of a single NV is well defined while the NVs in an ensemble have a range of depths.

In addition, an NV at a depth d below the diamond surface experiences a B_{RMS}^2 magnetic field from an external semi-infinite homogeneous layer of nuclei [48]:

$$B_{\text{RMS}}^2 = \rho \left(\frac{\mu_0 h \gamma_N}{4\pi} \right)^2 \left(\frac{\pi (8 - 3 \sin^4 \alpha)}{128 d^3} \right). \quad (23)$$

Here, μ_0 is the vacuum permeability, γ_N is the nuclear gyromagnetic ratio (in MHz/T), h is Planck's constant, ρ is the nuclear spin density, and α is the angle between the NV axis and the diamond surface normal vector. For NVs near a [100] diamond surface ($\alpha \approx 54.7^\circ$), which is the most common diamond surface cut, this reduces to

$$B_{\text{RMS}}^2 = \rho \left(\frac{\mu_0 h \gamma_N}{4\pi} \right)^2 \left(\frac{5\pi}{96 d^3} \right). \quad (24)$$

The signal-to-noise ratio (SNR) between η and the B_{RMS}^2 is an experimental figure-of-merit:

$$\text{SNR} = \frac{B_{\text{RMS}}^2}{\eta / \sqrt{s}}. \quad (25)$$

Maximizing the SNR (and minimizing the experiment duration) requires finding the depth for which an improvement in B_{RMS}^2 signal amplitude is worth the sacrifice in η . While η gets worse with shallower d , the B_{RMS}^2 amplitude improves with shallower d , as shown in Fig. 7 (a). To calculate η , we used a typical single-NV fluorescence intensity of $I_{PL} = 2 \times 10^5$ photons/s, $T_R = 10 \mu\text{s}$, $t_{int} = 2 \mu\text{s}$, and $A = 0.04$. To calculate B_{RMS}^2 and compare with Ref. [38], we used $\gamma_N = 13.66$ MHz/T, $\rho = 4.1 \times 10^{28}$ spins/m³ for ¹¹B in hBN, and $\gamma_e = 28$ GHz/T.

Figure 7 shows how η and B_{RMS}^2 vary with depth. Here we see that since B_{RMS}^2 decreases with depth more rapidly than η does, this means that a shallower depth should yield a better SNR. This result is consistent with experimental findings (e.g. Ref. [12, 38]), though we leave out additional depth-dependent phenomena that also affect η , such as NV conversion efficiency, photostability, I_{PL} , and A . In practice, these additional depth-dependent phenomena can spoil η faster than the $1/d^3$ B_{RMS}^2 improvement, meaning the depth for which the NV NMR spectroscopy SNR is maximized is greater than zero. A more complete analysis would include these effects, and is out of the scope of this current work.

This NV NMR spectroscopy example (statistically-polarized nuclei in a solid) does not necessarily generalize to every experimental situation. Applying this analysis to NV NMR spectroscopy of statistically-polarized nuclei

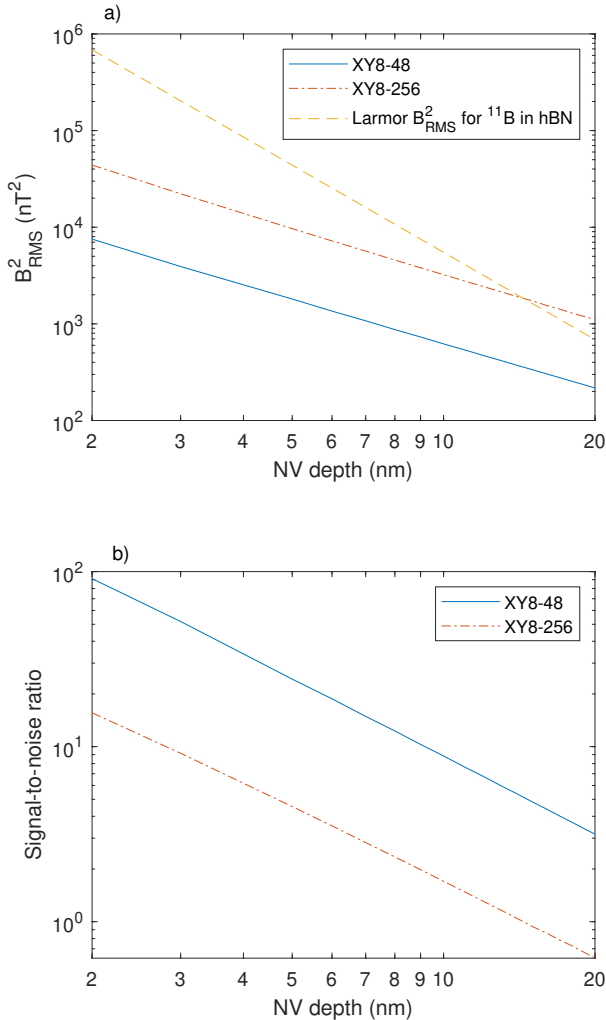


FIG. 7. (a) η/\sqrt{s} for XY8-48 (solid blue line), η/\sqrt{s} for XY8-256, (dashed-dotted red line), and Larmor B_{RMS}^2 for ¹¹B in hBN (dashed orange line) as a function of depth. B_{RMS}^2 improves with shallower depth like $1/d^3$, while the sensitivities get worse (though more slowly). (b) Signal-to-noise ratio (SNR) for XY8-48 (solid blue line) and XY8-256 (dashed-dotted red line). The SNR improves for shallower depths, though in practice other depth-dependent sensitivity factors (e.g. I_{PL}) move the SNR maximum to a depth greater than zero (e.g. 5.5 nm in Ref. [38]).

in a liquid (where the molecular diffusion time depends on NV depth), nuclei with a T_2^* much shorter than the NV T_2 , and thermally-polarized external nuclei will likely require modification of the above expressions for the appropriate depth-dependent SNR [53–55].

Note that we are modeling the worst-case scenarios for the noise sources. For example, we model the electric dipole noise considering a bare diamond as in Ref. [28]. In the actual experiments, there is a hydrocarbon layer

on the diamond surface, and the external nuclei on top of the hydrocarbon layer [38]. Depending on the surface dielectric, the surface electric dipole noise will change and the overall coherence time could increase, which will change the sensitivity.

V. CONCLUSIONS

The studies presented here have been threefold. First we investigated two noise sources due to the rough surface: the varying charge density which comes from electrons on the surface getting trapped within valley defects, and photons scattering incoherently from the rough surface. Second, we combined all our previous work on electric field noise and magnetic field noise with the rough surface noise and have done comprehensive analyses of the various noise effects on coherence times, $T_{2,\text{Hahn}}$ and T_2^* , and the longitudinal relaxation time, T_1 . Finally, we examined the NV AC magnetic sensing performance with depth and its trade-off compared to the magnetic field amplitude from external nuclei near the surface.

Our calculations of the varying charge density noise show the white noise present throughout the entire operational frequency range of 10³–10⁷ Hz due to the trapped electrons on the surface quickly beginning to fluctuate as they interact with each other. When considering a mostly smooth surface, the noise amplitude decreases considerably but still persists throughout the entire operational frequency range. This agrees with what has been seen in experiment before when using triacid-cleaning to get rid of the surface defects causing valleys [30]. As for the incoherent photon scattering noise due to the rough surface, the noise spectra show that the initialization and read-out pulses generate roughly 4–5 orders of magnitude more noise than the dynamical decoupling pulses. When compared to the other noise sources, the photon scattering is much weaker. When considering a wide range of rough surface correlation lengths we see that the rough surface is not impacting the photon scattering. **Methods such as fabricating photonic cavities to reduce the laser power required for initialization or photonic waveguides could help mitigate noise from photon scattering. It should be noted that if optically pumped within a resonant waveguide, the NVs will require less laser power but the photon rate and intensity at the NV will be the same.**

We combined this work with our previous work on electric field noise and magnetic field noise [27, 28] and examined the effect on coherence time. Our results gave that the surface magnetic impurities, electric dipole noise, and varying charge density noise play a large role in decreasing coherence times. We next calculated the surface noise effect on the longitudinal relaxation time T_1 , and verified that the result reflects experimentally determined values [11, 12] very well. When making our best assumptions to the possible noise sources in an experimental setup similar to Henshaw *et al.* [38] and assuming the scaling in the

coherence time due to the number of pulses [53], we saw good agreement for the coherence times for our range of depths when compared to their data.

With the comprehensive analysis on the noise effects on coherence times, we finally optimize the NV depth for magnetometry. Our SNR vs. depth assessment suggests that shallower NVs are better, a trend similar to what was seen by Henshaw *et al.* [38]. Since we only consider noise which we have modeled thus far, the difference in what we see compared to observed by their experiment comes from the fact that their measurements encompass everything that could be decreasing coherence times whereas we only look at one part of the whole picture. Our results show that the noise piece is an important one.

Again, it should be noted that our noise calculations do not account for various experimental efforts (e.g. tri-acid cleaning and annealing, choosing the correct protective layer, etc.) to reduce noise. However, our results give good predictions to what has been expected from these various noise sources and will aid experimental efforts. Regardless of the numerous experimental improvements to sensitivity, we still see that the noise is playing a major role in the decreasing of coherence times and among all our modeled noise sources, the surface noise is a major culprit. By reducing surface noise, extending lifetimes, and determining an optimal NV depth, one could increase the accuracy and fidelity of a wide range of NV sensing applications.

The predictions presented here can be improved by modeling additional noise sources, like electron spin noise from paramagnetic nitrogen defects (P1 centers) and possible electron-electron spin-spin interaction noise from the surface defects. The diamond ^{13}C isotopic abundance is also an important factor [27] that could modify the effects of some of our current models. Future work decomposing the components of each noise model can help us understand how the noise affects decoherence and relaxation separately, further strengthening the results presented here. Another future direction with these models could be the temperature dependence of the predicted coherence times, as each of the noise models we have described so far may have temperature dependence.

ACKNOWLEDGMENTS

This work is supported by the Advanced Quantum Sensing Center DoD contract W911NF2020276. We thank Andrew Mounce and Jacob Henshaw of Sandia National Laboratories for helpful discussions and experimental insights. Sandia National Laboratories is a multi-mission laboratory managed and operated by National Technology and Engineering Solutions of Sandia, LLC, a wholly owned subsidiary of Honeywell International,

Inc., for the DOE's National Nuclear Security Administration under contract DE-NA0003525. This paper describes objective technical results and analysis. Any subjective views or opinions that might be expressed in the paper do not necessarily represent the views of the U.S. Department of Energy or the United States Government.

Appendix A: Noise spectrum derivations

1. Varying charge density noise

To determine the areal charge density of the rough diamond surface due to defects, we use the Schottky approximation from the depletion of occupied states due to surface defects (which in diamond are usually primal $C = C$ sp² bonds [39]). The boundary conditions are:

$$\begin{aligned} \sigma(x) &= qN_A & 0 < x_d \leq x, \\ \sigma(x) &= 0 & x > x_d, \end{aligned} \quad (\text{A1})$$

where q is the electron charge, N_A is the defect concentration, and x_d is the length of the depletion region. The depletion region is the area where there is no moving charge so an electric field can be present. With these boundary conditions, the total charge per unit area within the depletion region is $Q_d = qN_A x_d$. The next step is to calculate the value for the length of the depleted region using experimentally available parameters. Gauss's law states

$$\oint E(x)dA = \frac{Q_d}{\varepsilon_s}, \quad (\text{A2})$$

where ε_s is the permittivity of the depleted region, E is the electric field, and dA is the differential area. From our boundary conditions for our charge density, we can determine how the electric field will look within our depleted region due to the defects as well as outside the region,

$$\begin{aligned} E(x) &= -\frac{qN_A}{\varepsilon_s}(x_d - x) & 0 < x < x_d, \\ E(x) &= 0 & x \geq x_d. \end{aligned} \quad (\text{A3})$$

Here the electric field goes to zero outside the depleted region. This makes sense as a non-zero field would cause mobile carriers to redistribute themselves until the field is zero. The maximum possible value for the electric field is $E_{\text{max}} = -qN_A x_d / \varepsilon_s$.

The electric potential corresponding to the electric field then becomes

$$\begin{aligned} \phi(x) &= 0 & x = 0, \\ \phi(x) &= \frac{qN_A}{2\varepsilon_s} [x_d^2 - (x_d - x)^2] & 0 < x < x_d, \\ \phi(x) &= \frac{qN_A}{2\varepsilon_s} x_d^2 & x > x_d. \end{aligned} \quad (\text{A4})$$

A boundary condition on the potential is applicable when the density of the free charge carriers is very high and the thickness of the charge layer is very thin, thus, a potential difference between them is orders of magnitude smaller than the potential difference within the defect despite the total amount of charge being the same. This is a key piece of the Schottky approximation and works well when determining the energy bands at the diamond surface. The total potential difference within the depletion region is the Fermi energy (E_F), that is further reduced or increased by the local energy level, E_n , in the depletion region. The boundary condition gives

$$E_F - E_n = -\phi(x=0) = \frac{qN_A x_d^2}{2\epsilon_s} \quad (\text{A5})$$

and the length of the depleted region becomes

$$x_d = \sqrt{\frac{2\epsilon_s(E_F - E_n)}{qN_A}}, \quad (\text{A6})$$

With the relation between the maximum electric field, we obtain the total charge per unit area which is similar to the approximation found in Ref. [39],

$$Q_d = \sqrt{qN_A 2\epsilon\epsilon_o(E_F - E_n)}. \quad (\text{A7})$$

where ϵ is the relative permittivity of diamond and ϵ_o is the permittivity of free space.

Using the total areal charge due to the surface defects, we now consider the time-dependent charge distribution as the defects trap mobile charges at the surface. Xia *et al.* [31] showed that the time-dependent charge concentration due to trapped electrons is

$$\sigma(t) = qN_{\text{trap}}f(E_n) \exp\left[-\int_0^t P_{\text{de}} dt'\right]. \quad (\text{A8})$$

Here q , N_{trap} , and $f(E_n)$, are the electron charge, trap density occupied, and the Fermi-Dirac distribution function at $t = 0$, respectively, and P_{de} is the probability of an electron being detrapped. The probability of an electron to be detrapped can be written as a Boltzmann rate,

$$P_{\text{de}} = v_{\text{de}} \exp\left[-\frac{E_T}{k_B T}\right], \text{ where } v_{\text{de}} = \frac{(k_B T)^3}{6h^3 v^2}.$$

Here v_{de} is the maximum detrapping rate, k_B is Boltzmann's constant, T is temperature, h is Planck's constant, and v is the orthogonal vibrational frequency around the defect. The energy level of the traps is temperature- and time-dependent and is represented by $E_T = k_B T \ln(v_{\text{de}} t)$. Plugging in the definition of E_T and v_{de} into P_{de} makes determining the probability of detrapping a straight forward process and gives the the time-dependent charge concentration as

$$\sigma(t) = qN_{\text{trap}}f(E_n) \exp\left[-\frac{v_{\text{de}}^2 t^2}{2}\right], \quad (\text{A9})$$

$$\text{where } f(E_n) = \left[1 + \exp\left(\frac{E_F - E_n}{k_B T}\right)\right]^{-1}.$$

Assuming that q is the total charge at $t = 0$, q will now be replaced by the total charge per unit area due to the defects causing roughness, $Q_d = \sqrt{qN_A 2\epsilon\epsilon_o(E_F - E_n)}$. Plugging in the total charge per unit area from before we get the following time-dependent charge density,

$$\sigma(t) = Q_d N_{\text{trap}} f(E_n) \exp\left[-\frac{v_{\text{de}}^2 t^2}{2}\right]. \quad (\text{A10})$$

With the time dependence of the charge density, the two-time correlation can be expressed by an auto-correlation function of the time-dependent charge density

$$\langle \delta\sigma(t), \delta\sigma(t + \tau) \rangle = \Lambda \frac{\exp\left[\frac{v_{\text{de}}^2 \tau^2}{4}\right] \sqrt{\pi}}{v_{\text{de}}}, \quad (\text{A11})$$

$$\text{where } \Lambda = Q_d^2 N_{\text{trap}}^2 f(E_n)^2 \exp\left[-\frac{v_{\text{de}}^2 \tau^2}{2}\right].$$

The auto-correlation function can then be plugged into the Wiener-Khinchin theorem to relate to the noise spectral density,

$$S_{CD}(\omega) = \int_{-\infty}^{\infty} \langle \delta\sigma(t), \delta\sigma(t + \tau) \rangle \exp[-i\omega\tau] d\tau.$$

After applying the Wiener-Khinchin theorem, we get the noise power density,

$$S_{CD}(\omega) = Q_d^2 N_{\text{trap}}^2 f(E_n)^2 \frac{\exp\left[-\frac{\omega^2}{v_{\text{de}}^2}\right] \sqrt{2\pi}}{v_{\text{de}}^2}. \quad (\text{A12})$$

2. Incoherent photon scattering

a. Green's function method

As photons from the initialization, readout, and Hahn echo pulses interact with the diamond substrate, atoms within the diamond will have elastic collisions with incoming photons. The atoms will vibrate emitting electromagnetic radiation. This requires knowing the fields radiated from the scattering. We approach this by considering the Green's function method applied to the wave equation. The potentials from the pump laser pulse can usually be considered from the Lorenz gauge or Gaussian. Either way the wave equation will take the following form,

$$\nabla^2 \Phi - \frac{1}{c^2} \frac{\partial^2 \Phi}{\partial t^2} = -4\pi. \quad (\text{A13})$$

Here Φ can be either a scalar potential or a component of the potential. This gives the corresponding Green's function equation,

$$\nabla^2 G(\vec{x}, t; \vec{x}', t') - \frac{1}{c^2} \frac{\partial^2 G}{\partial t^2} = -4\pi \delta(\vec{x} - \vec{x}') \delta(t - t'), \quad (\text{A14})$$

where the source is now an event located at $\vec{x} = \vec{x}'$ happening at $t = t'$. Performing a Fourier transform and considering the spherical symmetry and the properties of the delta function give a solution for the Green's function Fourier transform,

$$G(\vec{x}, \omega; \vec{x}', t') = \frac{1}{\sqrt{2\pi R}} (Ae^{ikR} + Be^{-ikR}) e^{-i\omega t'}. \quad (\text{A15})$$

Doing the inverse transform to get us back our original Green's function,

$$G(\vec{x}, t; \vec{x}', t') = \frac{1}{\sqrt{2\pi}} \int_{-\infty}^{\infty} G(\vec{x}, \omega; \vec{x}', t') e^{-i\omega t} d\omega, \quad (\text{A16})$$

$$G(\vec{x}, t; \vec{x}', t') = A\delta(t' - (t - \frac{R}{c})) + B\delta(t' - (t + \frac{R}{c})). \quad (\text{A17})$$

The second term is usually rejected as it predicts a response to an event occurring in the future, so here we shall do the same. The time $t - R/c$ here is normally referred to as the retarded time t_{ret} . With our Green's function we can solve our wave equation and determine the potential,

$$\Phi(\vec{x}, t) = \frac{1}{c} \int \frac{\vec{j}(\vec{x}', t')}{R} \delta(t' - t_{ret}) dt' d^3x', \quad (\text{A18})$$

$$\Phi(\vec{x}, t) = \frac{1}{c} \int \frac{\vec{j}(\vec{x}', t_{ret})}{R} d^3x'. \quad (\text{A19})$$

It can be seen relatively easily that this represents a static potential, but for our case we want the field from a charge that is accelerating due to it interacting with the photon.

b. Scattered field solution

Our source of the scattered field is going to be an atom, more specifically a charge, accelerating due to the elastic collision with the incoming photon. This will allow us to rewrite Eq. (A19) as the following,

$$\Phi(\vec{x}, t) = \frac{1}{c} \int \frac{q\vec{v}\delta(\vec{x}' - \vec{r}(t'))}{R} \delta(t' - t_{ret}) dt' d^3x'. \quad (\text{A20})$$

Here \vec{v} is the velocity of the oscillating charge and $\vec{r}(t')$ is the position changing over time. Doing the integral over the spatial coordinates we get,

$$\Phi(\vec{x}, t) = \frac{1}{c} \int q\vec{v} \frac{\delta(t' + R(t')/c - t)}{R(t')} dt', \quad (\text{A21})$$

where $R(t') = |\vec{x}' - \vec{r}(t')|$. With what we have here, we cannot do a straight integration of t' . We will have to reexpress the delta function to do this integral to be the delta function of a function which has the form,

$$\delta(f(t')) = \sum \frac{1}{|f'(t'_i)|} \delta(t' - t'_i). \quad (\text{A22})$$

where $f(t'_i) = 0$. Taking the derivative and using the definition of the velocity, we will get,

$$f'(t'_i) = 1 + \frac{1}{c} \frac{dR}{dt'} = 1 - \frac{1}{c} \frac{(\vec{x} - \vec{r}(t'))}{|\vec{x} - \vec{r}(t')|} \cdot \frac{d}{dt'} (\vec{x} - \vec{r}(t')), \quad (\text{A23})$$

$$f'(t'_i) = 1 - \frac{\vec{v} \cdot (\vec{x} - \vec{r}(t'))}{c|\vec{x} - \vec{r}(t')|} = 1 - \frac{\vec{v} \cdot \vec{R}}{cR}. \quad (\text{A24})$$

This function is zero for $t = t_{ret}$, so evaluating the integrals we get

$$\Phi(\vec{x}, t) = \frac{q\vec{v}}{R(1 - \frac{\vec{v} \cdot \vec{R}}{cR})}. \quad (\text{A25})$$

This is the Leinhard-Wiechart potential, and from here we can start determining the scattering field.

The electric field from electromagnetic radiation is proportional to the magnetic field as $\vec{B} = \vec{E}c$. From this, the field which will have the largest interaction with the NV center electron spin will be the electric field. Thus, we only consider the electric field emitted from the Rayleigh scattering within the diamond lattice. We can write the electric field as follows:

$$\vec{E}(\vec{x}, t) = -\vec{\nabla}V - \frac{1}{c} \frac{\partial \vec{\Phi}}{\partial t}, \quad (\text{A26})$$

where the potential V looks like $\Phi(\vec{x}, t)$ without the velocity factor. The potentials here are in terms of \vec{x} and t_{ret} , so the partial derivatives will be a bit different, but we can put the origin at the spontaneous position of the oscillating charge, $R = r$, allowing us to simplify things. Rewriting the electric field to fit our potentials in terms of \vec{x} and t_{ret} we get

$$\vec{E}(\vec{x}, t_{ret}) = \vec{\nabla}V \cdot d\vec{x} - \frac{\partial \vec{\Phi}}{\partial t_{ret}} \frac{dr}{c} + \frac{\partial \vec{\Phi}}{\partial t_{ret}} dt. \quad (\text{A27})$$

Looking at the first term of the electric field we get,

$$\vec{\nabla}V = \vec{\nabla} \frac{q}{r} = -\frac{q}{r^2} \vec{\nabla}r, \quad (\text{A28})$$

where

$$\vec{\nabla}r = \quad (\text{A29})$$

$$\frac{\partial}{\partial r} \left(r - \frac{\vec{r} \cdot \vec{v}}{c} \right) \hat{r} + \frac{\hat{\theta}}{r} \frac{\partial}{\partial \theta} \left(r - \frac{\vec{r} \cdot \vec{v}}{c} \right) + \frac{\hat{\phi}}{r \sin \theta} \frac{\partial}{\partial \phi} \left(r - \frac{\vec{r} \cdot \vec{v}}{c} \right).$$

Choosing our axes with polar axis along the instantaneous direction of the velocity, we get $\vec{r} \cdot \vec{v} = rv \cos \theta$ giving us,

$$\vec{\nabla}r = \left(1 - \frac{v}{c} \cos \theta \right) \hat{r} + \frac{\hat{\theta}}{r} \left(r \frac{v}{c} \sin \theta \right). \quad (\text{A30})$$

We can consider here the non-relativistic limit such that $v/c \ll 1$, simplifying the first term in our electric field to be $\vec{\nabla}r = \hat{r}$. To get the entire electric field, we will need the $\partial r/\partial t$ term, which will simply give $\partial r/\partial t = -(\vec{r} \cdot \vec{a})/c$. Putting everything together, we have

$$\vec{E} = \frac{q}{r^2} \hat{r} \left(1 + \frac{(\vec{r} \cdot \vec{a})}{c} \right) - \frac{q\vec{a}}{cr} + \frac{q\vec{v}}{cr^2} \left(r - \frac{(\vec{r} \cdot \vec{a})}{c} \right), \quad (\text{A31})$$

$$\vec{E} = \frac{q}{r^2} \hat{r} \left(1 + \frac{(\vec{r} \cdot \vec{a})}{c} \right) - \frac{q\vec{a}}{cr}. \quad (\text{A32})$$

The first term is the usual point charge term, but the other two terms are the radiated field.

You can also look at the trigonometry and see that the parallel component is the piece that resembles a static charge where as the emitted field will then be the perpendicular piece. Doing the full vector analysis, we will get the radiated component of the electric field,

$$E(t) = \frac{qa(t) \sin(\theta)}{4\pi\epsilon_0rc^2}. \quad (\text{A33})$$

Here q is the electron charge, ϵ_0 is the permittivity of free space, r is the radial distance from the electron, $a(t)$ is the vibrational acceleration of the charge, θ is the scattering angle, and c is the speed of light. We neglect the static field term as physically its interaction with the NV center electron will be much smaller that of the emitted field from the oscillating charge, so it will not add to the noise.

c. Rayleigh scattering noise density

Now that we have the emitted field due to the scattering, we need to determine the acceleration of the oscillating charge. We can do this by considering the position of an electron bound to an atom in an applied oscillating electric field,

$$x_e(t) = \frac{qE_0}{m_e(\omega_0^2 - \omega_{\text{inc}}^2)} \exp[-i\omega_{\text{inc}}t]. \quad (\text{A34})$$

Here E_0 is the amplitude of the electric field, m_e is the mass of the electron, ω_0 is the resonant frequency of the diamond, and ω_{inc} is the frequency of the oscillating field (incident light-wave). For both pulses, $\omega_{\text{inc}} \gg \omega_0$, and from this we get the acceleration of the oscillating charge will be

$$a(t) = -\frac{qE_0}{m_e} \exp[-i\omega_{\text{inc}}t]. \quad (\text{A35})$$

It is important to note that the Hahn echo pulse could be near this resonant (microwave) frequency, possibly blowing up the above expression, but if we calculate E_0 from experimental values we will get an extremely small amplitude counteracting this large value from $1/(\omega_0^2 - \omega_{\text{inc}}^2)$

leading to a small acceleration. From this we will continue with what is derived here, as the method will not change.

Now that we have a time-dependent electric field, we can determine the two-time correlation function. One constraint to place is that at $t < 0$ the correlation will go to zero when considering causality. This can also be done as to determine our potentials the Green's function required a similar causality. This will allow us to shift the integration limits for the correlation function integration as well as deal with any convergence issues of the exponential function. The two-time correlation function is then defined as

$$\langle E(t)E(t+\tau) \rangle = E(\theta) \int_0^\infty e^{[-i\omega_{\text{inc}}t]} e^{[-i\omega_{\text{inc}}(t+\tau)]} d\tau, \quad (\text{A36})$$

$$\text{where } E(\theta) = \frac{q^2 E_0 \sin(\theta)}{m_e 4\pi \epsilon_0 r c^2}$$

$$\langle E(t)E(t+\tau) \rangle = E(\theta)^2 \frac{\exp[-i\omega_{\text{inc}}\tau]}{2\omega_{\text{inc}}}. \quad (\text{A37})$$

With the two-time correlation function, we can apply the Wiener-Khinchin theorem and the same causality constraint as before to shift the integration limits and get rid of any convergence issues to get the noise spectral density,

$$S_{RS}(\omega) = \int_0^\infty \langle E(t)E(t+\tau) \rangle \exp[-i\omega\tau] d\tau, \quad (\text{A38})$$

$$S_{RS}(\omega) = E(\theta)^2 \frac{1}{2\omega_{\text{inc}}(\omega_{\text{inc}} + \omega)}. \quad (\text{A39})$$

d. Rough surface scattering density

To characterize rough surface causing photon scattering, we need a correlation function to describe the surface roughness. In this sense, we will describe the rough surface correlation as

$$C(R) = \frac{1}{\sigma^2} \langle h(r)h(r+R) \rangle, \quad (\text{A40})$$

where $h(r)$ is the surface height a distance r away from a smooth reference plane and σ is the root-mean-square height. Here we use a Gaussian correlation function of the rough surface. It should be noted that the correlation function can also be described with an exponential, which data is often fit to.

To see how the surface roughness will effect the noise due to scattering, we need to generate the power spectrum of the rough surface by taking the Fourier transform

$$P(k) = \frac{\sigma^2}{(2\pi)^2} \int_{-\infty}^\infty C(R) \exp(ik \cdot R) dR. \quad (\text{A41})$$

Here k is the wave number and is related to the frequency of the scattered wave by $k = \omega/c$. Plugging in the Gaussian correlation functions and doing the integral, we get following power density

$$P_G(\omega) = \frac{\sigma^2 \lambda}{4\pi^{2/3}} \exp\left(\frac{\lambda^2 \omega^2}{4c^2}\right), \quad (\text{A42})$$

where λ is the correlation length. Now that we have

the rough surface, we need to combine our noise and rough surface power densities to generate the actual photon scattering noise power spectral density seen by the NV center spin giving us

$$S_{RS}(\omega) = P_G(\omega) E(\theta)^2 \frac{1}{2\omega_{\text{inc}}(\omega_{\text{inc}} + \omega)}. \quad (\text{A43})$$

-
- [1] L. Childress, R. Walsworth, and M. Lukin, Atom-like crystal defects: From quantum computers to biological sensors, *Physics Today* **67** (10), 38 (2014).
- [2] Z. Xiang, S. Ashhab, J. Q. You, and F. Nori, Hybrid quantum circuits: Superconducting circuits interacting with other quantum systems, *Rev. Mod. Phys.* **86**, 623 (2013).
- [3] R. Schirhagl, K. Chang, M. Loretz, and C. L. Degen, Nitrogen-Vacancy Centers in Diamond: Nanoscale Sensors for Physics and Biology, *Annual Review of Physical Chemistry* **65** (1), 83-105 (2014).
- [4] J. F. Barry, J. M. Schloss, E. Bauch, M. J. Turner, C. A. Hart, L. M. Pham, and R. L. Walsworth, Sensitivity optimization for NV-diamond magnetometry, *Rev. Mod. Phys.* **92**, 015004 (2020).
- [5] T. Staudacher, F. Shi, S. Pezzagna, J. Meijer, J. Du, C. A. Meriles, F. Reinhard, and J. Wrachtrup, Nuclear Magnetic Resonance Spectroscopy on a (5-Nanometer)³ Sample volume, *Science* **339** (6119), 561 (2013).
- [6] D. Rugar, H. J. Mamin, M. H. Sherwood, M. Kim, C. T. Rettner, K. Ohno, and D. D. Awschalom, Proton magnetic resonance imaging using a nitrogen-vacancy spin sensor, *Nat. Nanotechnol.* **10**, 120 (2015).
- [7] T. Häberle, D. Schmid-Lorch, F. Reinhard, and J. Wrachtrup, Nanoscale nuclear magnetic imaging with chemical contrast, *Nat. Nanotechnol.* **10**, 125 (2015).
- [8] M. Kim, H. J. Mamin, M. H. Sherwood, C. T. Rettner, J. Frommer, and D. Rugar, Ultrafast magnetization switching by spin-orbit torques, *Appl. Phys. Lett.* **105**, 042406 (2014).
- [9] M. Kim, H. J. Mamin, M. H. Sherwood, K. Ohno, D. D. Awschalom, and D. Rugar, Decoherence of Near-Surface Nitrogen-Vacancy Centers Due to Electric Field Noise, *Phys. Rev. Lett.* **115**, 087602 (2015).
- [10] F. Fávoro de Oliveira, S. Momenzadeh, D. Antonov, H. Fedder, A. Denisenko, and J. Wrachtrup, On the efficiency of combined ion implantation for the creation of near-surface nitrogen-vacancy centers in diamond, *Phys. Status Solidi*, **8** 2044-2050 (2016).
- [11] B. A. Myers, A. Ariyaratne, and A. C. Bleszynski Jayich, Double-Quantum Spin-Relaxation Limits to Coherence of Near-Surface Nitrogen-Vacancy Centers, *Phys. Rev. Lett.* **118**, 197201 (2017).
- [12] B. A. Myers, A. Das, M. C. Dartiaillh, K. Ohno, D. D. Awschalom, and A. C. Bleszynski Jayich, Probing Surface Noise with Depth-Calibrated Spins in Diamond, *Phys. Rev. Lett.* **113**, 027602 (2014).
- [13] T. Rosskopf, A. Dussaux, K. Ohashi, M. Loretz, R. Schirhagl, H. Watanabe, S. Shikata, K. M. Itoh, and C. L. Degen, Investigation of Surface Magnetic Noise by Shallow Spins in Diamond, *Phys. Rev. Lett.* **112**, 147602 (2014).
- [14] B. K. Ofori-Okai, S. Pezzagna, K. Chang, M. Loretz, R. Schirhagl, Y. Tao, B. A. Moores, K. Groot-Berning, J. Meijer, and C. L. Degen, Spin properties of very shallow nitrogen vacancy defects in diamond, *Phys. Rev. B* **86**, 081406(R) (2012).
- [15] Rogerio De Sousa, Dangling-bond spin relaxation and magnetic 1/f noise from the amorphous-semiconductor/oxide interface: Theory, *Phys. Rev. B* **76**, 245306 (2007).
- [16] N. Bar-Gill, L. Pham, C. Belthangady, D. Le Sage, P. Cappellaro, J. Maze, M. Lukin, A. Yacoby, and R. Walsworth, Suppression of spin-bath dynamics for improved coherence of multi-spin-qubit systems, *Nat. Commun.* **3**, 858 (2012).
- [17] N. Bar-Gill, L.M. Pham, A. Jarmola, D. Budker, and R. L. Walsworth, Solid-state electronic spin coherence time approaching one second, *Nat. Commun.* **4**, 1743 (2013).
- [18] V. Y. Osipov, A. Shames, and A. Y. Vul, Exchange coupled pairs of dangling bond spins as a new type of paramagnetic defects in nanodiamonds, *Physica (Amsterdam)* **404B**, 4522 (2009).
- [19] N. D. Samsonenko, G. V. Zhmykhov, V. S. Zon, and V. K. Aksenov, Characteristic features of the electron paramagnetic resonance of the surface centers of diamond, *J. Struct. Chem.* **20**, 951 (1980).
- [20] J. Tisler, G. Balasubramanian, B. Naydenov, R. Kolesov, B. Grotz, R. Reuter, J. P. Boudou, P. A. Curmi, M. Sennour, A. Thorel, M. Börsch, K. Aulenbacher, R. Erdmann, P. R. Hemmer, F. Jelezko, and J. Wrachtrup, Fluorescence and Spin Properties of Defects in Single Digit Nanodiamonds, *ACS Nano* **3**, 1959 (2009).
- [21] L. P. McGuinness, L. T. Hall, A. Stacey, D. A. Simpson, C. D. Hill, J. H. Cole, K. Ganesan, B. C. Gibson, S. Praver, P. Mulvaney, F. Jelezko, J. Wrachtrup, R. E. Scholten, and L. C. L. Hollenberg, Ambient nanoscale sensing with single spins using quantum decoherence, *New. J. Phys.* **15**, 073042 (2013).
- [22] R. C. Bansal, F. J. Vastola, and P. L. Walker, Kinetics of chemisorption of oxygen on diamond, *Carbon* **10**, 443 (1972).
- [23] H. Bluhm, J. A. Bert, N. C. Koshnick, M. E. Huber, and K. A. Moler, Spinlike Susceptibility of Metallic and Insulating Thin Films at Low Temperature, *Phys. Rev. Lett.* **103**, 026805 (2009).
- [24] F. Pierre, A. B. Gougam, A. Anthore, H. Pothier, D. Esteve, and N. O. Birge, *Phys. Rev. B* **68**, 085413 (2003).
- [25] K. Ohashi, T. Rosskopf, H. Watanabe, M. Loretz, Y. Tao, R. Hauert, S. Tomizawa, T. Ishikawa, J. Ishi-Hayase, S. Shikata, C. L. Degen, and K. M. Itoh, Negatively Charged Nitrogen-Vacancy Centers in a 5 nm Thin ¹²C

- Diamond Film, *Nano Lett.* **13** (10), 4733 (2013).
- [26] K. Ohno, F. Joseph Heremans, L. C. Bassett, B. A. Myers, D. M. Toyli, A. C. Bleszynski Jayich, C. J. Palmstrom, and D. D. Awschalom, Engineering shallow spins in diamond with nitrogen delta-doping, *Appl. Phys. Lett.* **101**, 082413 (2012).
- [27] P. Chrostoski, B. Barrios, and D. H. Santamore, Magnetic field noise analyses generated by the interactions between a nitrogen vacancy center diamond and surface and bulk impurities, *Physica B: Condensed Matter* **605**, 412767 (2021).
- [28] P. Chrostoski, H.R. Sadeghpour, and D.H. Santamore, Electric noise spectra of a near-surface nitrogen vacancy center diamond with a protective layer, *Phys. Rev. Appl.* **10**, 064056 (2018).
- [29] K. C. Miao, J. P. Blanton, C. P. Anderson, A. Bourassa, A. L. Crook, G. Wolfowicz, H. Abe, T. Ohshima, and D. D. Awschalom, *Science* **369**, 1493-1497 (2020).
- [30] S. Sangtawesin, B. L. Dwyer, S. Srinivasan, J. J. Allred, L. V. H. Rodgers, K. De Greve, A. Stacey, N. Dontschuk, K. M. O'Donnell, D. Hu, D. A. Evans, C. Jaye, D. A. Fischer, M. L. Markham, D. J. Twitchen, H. Park, M. D. Lukin, and N. P. de Leon, Origins of Diamond Surface Noise Probed by Correlating Single-Spin Measurements with Surface Spectroscopy, *Phys. Rev. X* **9**, 031052 (2019).
- [31] J. Li, F. Zhou, D. Min, S. Li and R. Xia, The energy distribution of trapped charges in polymers based on isothermal surface potential decay model, *IEEE Transactions on Dielectrics and Electrical Insulation* **22** (3), 1723-1732 (2015).
- [32] M. Constantin, C. C. Yu, and J. M. Martinis, Saturation of two-level systems and charge noise in Josephson junction qubits, *Phys. Rev. B* **79**, 094520 (2009).
- [33] J. Bergli, Y. M. Galperin, and B. L. Altshuler, Decoherence in qubits due to low-frequency noise, *New J. Phys.* **11**, 025002 (2009).
- [34] S. M. Kogan, *Electronic Noise and Fluctuations in Solids*, Cambridge University Press (1996).
- [35] R. Sahay, S. Hsieh, E. Parsonnet, L. W. Martin, R. Ramesh, N. Y. Yao, and S. Chatterjee, Noise Electrometry of Polar and Dielectric Materials, arXiv:2111.09315 (2021).
- [36] Y. Romach, C. Müller, T. Unden, L. J. Rogers, T. Isoda, K. M. Itoh, M. Markham, A. Stacey, J. Meijer, S. Pezagna, B. Naydenov, L. P. McGuinness, N. Bar-Gill, and F. Jelezko, Spectroscopy of Surface-Induced Noise Using Shallow Spins in Diamond, *Phys. Rev. Lett.* **114**, 017601 (2015).
- [37] J. R. Maze, P. L. Stanwix, J. S. Hodges, S. Hong, J. M. Taylor, P. Cappellaro, L. Jiang, M. V. Gurudev Dutt, E. Togan, A. S. Zibrov, A. Yacoby, R. L. Walsworth, and M. D. Lukin, Nanoscale magnetic sensing with an individual electronic spin in diamond, *Nature* **455**, 644-647 (2008).
- [38] J. Henshaw, P. Kehayias, M. S. Ziabari, M. Titze, E. Morissette, K. Watanabe, T. Taniguchi, J.I.A Li, V. M. Acosta, E. Bielejec, M. P. Lilly, and A. M. Mounce, Nanoscale Solid-State Nuclear Quadrupole Resonance Spectroscopy using Depth-Optimized Nitrogen-Vacancy Ensembles in Diamond, *Appl. Phys. Lett.* **120**, 174002 (2022).
- [39] A. Stacey, N. Dontschuk, J.-P. Chou, D. A. Broadway, A. K. Schenk, M. J. Sear, J.-P. Tetienne, A. Hoffman, S. Praver, C. I. Pakes, A. Tadich, N. P. de Leon, A. Gali, and L. C. L. Hollenberg, Evidence for Primal sp^2 Defects at the Diamond Surface: Candidates for Electron Trapping and Noise Sources, *Adv. Mater. Interfaces* **6**, 1801449 (2019).
- [40] The Element Six, see <http://www.e6cvd.com/> for CVD Diamond Handbook.
- [41] S. D. Subedi, V. V. Fedorov, J. Peppers, D. V. Martyshkin, S. B. Mirov, L. Shao and Ma. Loncar, Laser spectroscopy of highly doped NV- centers in diamond, *Proc. SPIE 10511, Solid State Lasers XXVII: Technology and Devices*, 105112D (2018).
- [42] T.-L. Wee, Y.-K. Tzeng, C.-C. Han, H.-C. Chang, W. Fann, J.-H. Hsu, K.-M. Chen, and Y.-C. Yu, Two-photon Excited Fluorescence of Nitrogen-Vacancy Centers in Proton-Irradiated Type Ib Diamond, *J. Phys. Chem. A* **111**, 9379-9386 (2007).
- [43] R. Chapman and T. Plakhotnik, Quantitative luminescence microscopy on Nitrogen-Vacancy Centres in diamond: Saturation effects under pulsed excitation, *Chemical Physics Letters* **507**, 190-194 (2011).
- [44] P. H. Handel, $1/f$ Noise - An "Infrared" Phenomena, *Phys. Rev. Lett.* **34**, 1492 (1975).
- [45] P. H. Handel, Quantum approach to $1/f$ noise, *Phys. Rev. A* **22**, 745 (1980).
- [46] G.S. Kousik, C.M. Van Vliet, G. Bosman, and P. H. Handel, Quantum $1/f$ noise associated with ionized impurity scattering and electron-phonon scattering in condensed matter, *Advances in Physics* **34**, 663-702 (1985).
- [47] M. Mihaila, D. Ursutiu, and I. Sandu, Electron-Phonon Coupling as the Source of $1/f$ Noise in Carbon Soot, *Sci. Rep.* **9**, 947 (2019).
- [48] L. M. Pham, S. J. DeVience, F. Casola, I. Lovchinsky, A. O. Sushkov, E. Bersin, J. Lee, E. Urbach, P. Cappellaro, H. Park, A. Yacoby, M. Lukin, and R. L. Walsworth, NMR technique for determining the depth of shallow nitrogen-vacancy centers in diamond, *Phys. Rev. B* **93**, 045425 (2016).
- [49] A. M. Souza, G. A. Álvarez, and D. Suter, "Robust dynamical decoupling," *Philosophical Transactions of the Royal Society A: Mathematical, Physical and Engineering Sciences* **370**, 4748-4769 (2012).
- [50] B. Naydenov, F. Dolde, L. T. Hall, C. Shin, H. Fedder, L. C. L. Hollenberg, F. Jelezko, and J. Wrachtrup, Dynamical decoupling of a single-electron spin at room temperature, *Phys. Rev. B* **83**, 081201(R) (2011).
- [51] A. Jarmola, V. M. Acosta, K. Jensen, S. Chemerisov, and D. Budker, Temperature- and Magnetic-Field-Dependent Longitudinal Spin Relaxation in Nitrogen-Vacancy Ensembles in Diamond, *Phys. Rev. Lett.* **108**, 197601 (2012).
- [52] L. T. Hall, P. Kehayias, D. A. Simpson, A. Jarmola, A. Stacey, D. Budker, L. C. L. Hollenberg, Detection of nanoscale electron spin resonance spectra demonstrated using nitrogen-vacancy centre probes in diamond, *Nat. Commun.* **7**, 10211 (2016).
- [53] P. Kehayias, A. Jarmola, N. Mosavian, I. Fescenko, F. M. Benito, A. Laraoui, J. Smits, L. Bougas, D. Budker, A. Neumann, S. R. J. Brueck, and V. M. Acosta, Solution nuclear magnetic resonance spectroscopy on a nanostructured diamond chip, *Nat. Commun.* **8**, 188 (2017).
- [54] D. R. Glenn, D. B. Bucher, J. Lee, M. D. Lukin, H. Park, and R. L. Walsworth, High-resolution magnetic resonance spectroscopy using a solid-state spin sensor,

- Nature **555**, 351-354 (2018).
- [55] J. Smits, J. Damron, P. Kehayias, A. F. McDowell, N. Mosavian, I. Fescenko, N. Ristoff, A. Laraoui, A. Jarmola, and V. M. Acosta, Two-dimensional nuclear magnetic resonance spectroscopy with a microfluidic diamond quantum sensor, *Sci. Adv.* **5** 7, eaaw7895 (2019).